Supplementary Information

Dual-Carbon and Chalcogenide Engineered Ni_3Se_4/Delaminated V_2C MXene /reduced Graphene Oxide Composite as the Bifunctional Electrode for Asymmetric Supercapacitor and Hydrogen Evolution Applications

Johnbosco Yesuraj[a1], Erdenebayar Baasanjav[a1], Hafis Hakkeem[a], Chandra Sekhar Rout[a c*], Sang Mun Jeong [a b*]

[a]Department of Chemical Engineering, Chungbuk National University, 1 Chungdae-ro, Seowon-Gu, Cheongju, Chungbuk, 28644, Republic of Korea

[b]Advanced Energy Research Institute, Chungbuk National University, 1 Chungdae-ro, Seowon-Gu, Cheongju, Chungbuk, 28644, Republic of Korea

[c]Centre for Nano and Material Sciences, Jain University, Jain Global Campus, Jakkasandra, Ramanagaram, Bangalore, 562112, India

Corresponding authors*: r.chandrasekhar@jainuniversity.ac.in (C. S. Rout) and smjeong@chungbuk.ac.kr (S. M. Jeong)

[1] These authors equally contributed to this work

1. Materials

Nickel chloride hexahydrate ($NiCl_2.6H_2O$), Hydrazine monohydrate ($N_2H_4.\ H_2O$) Sodium selenate (Na_2SeO_3) Potassium Permanganate ($KMnO_4$), Tetramethylammonium hydroxide solution ($(CH_3)_4NOH$, TMAOH, 25 wt.% in water), L-ascorbic acid ($C6H_8O_6$), N-Methyl-2-pyrrolidone (NMP, C_5H_9NO, ≥99.5%), activated carbon, and Poly(vinylidene fluoride) (PVDF) were procured from Sigma-Aldrich company. Vanadium aluminium carbide (V_2AlC, MAX phase) was purchased from Laizhou Kai Kai Ceramic Materials Co., Ltd (China). Hydrofluoric acid (HF), Sulfuric acid (H_2SO_4) and hydrochloric acid HCl (37 wt% %, 12.17 M) were obtained from Thermo Fisher Scientific company. The Graphite and ethyl alcohol were supplied by Samchun Chemicals. All chemicals were of analytical grade and used as received without further purification, and deionized (DI) water was used in all experiments.

2. Synthesis section

Table S1: The weight percentage of composites

S. No	Material	Ni_3Se_4 (Weight%)	V_2C (Weight%)	GO (Weight%)
1	Ni_3Se_4	100 % (0.69 g)	-	-
2	$Ni_3Se_4V_2C$	90 % (0.69 g)	10 % (0.076 g)	-
3	Ni_3Se_4/rGO	90 % (0.69 g)	-	10 % (0.076 g)
4	Ni_3Se_4/V_2C/rGO	90 % (0.69 g)	5 % (0.038 g)	5 % (0.038g)

In Table S1, the mass of Ni_3Se_4 (0.69 g) was taken as the reference value, corresponding to 90 wt% of the total composite. This baseline was consistently applied for the preparation of three different composite systems: $Ni_3Se_4V_2C$, Ni_3Se_4/rGO, and Ni_3Se_4/V_2C/rGO composites.

3. Material characterizations

The crystal structure analyses were carried out with an X-ray diffractometer (XRD) using D8 Discover with GADDS and Cu Kα radiation (α -1.54 Å) and Raman spectroscopy (excitation at 532 nm, RAMANtouch, Nanophoton). A field-emission scanning electron microscope (FE-SEM, ULTRA PLUS, ZEIS) and a transmission electron microscope (JEOL; JEM-ARM200F) were employed to investigate the microstructures of all materials. The oxidation state of the materials was evaluated using X-ray photoelectron spectroscopy (XPS) (PHI Quantera-II, Al Kα radiation, Ulvac-PHI. Nitrogen adsorption/desorption isotherms were conducted at 77 K for all materials to evaluate surface areas and pore size distribution characteristics. These measurements were performed using the Brunauer–Emmett–Teller (BET) method and the Barrett-Joyner-Halenda (BJH) method, respectively, with nitrogen as the adsorbate gas.

4. Electrode preparation for supercapacitor analysis

The working electrodes were prepared using a slurry-coating process. The NMP (N-methyl-2-pyrrolidone) solvent was used to make the slurry, which was composed of 80% active material (Ni_3Se_4, Ni_3Se_4/V_2C, Ni_3Se_4/rGO, and Ni_3Se_4/V_2C/rGO composite), 10% PVDF (polyvinylidene fluoride) as a binder, and 10% carbon black as a conducting agent. This slurry was evenly applied to a current collector made of 1 x 1 cm Nickel foam. Prior to the coating process, the nickel foam was pretreated by immersion in diluted hydrochloric acid to remove surface oxides and impurities, followed by thorough rinsing with DI water to ensure a clean and contaminant-free surface. The resultant electrodes were dried in a vacuum oven at 80 °C for 12 h. The resulting electrode contained an active material weighing approximately 4.5 mg. All the supercapacitor electrochemical experiments were conducted using the Metrohm Autolab Instrument. Furthermore, three-electrode and asymmetric device experiments were conducted using a 2 M KOH electrolyte. A platinum sheet was used as the counter electrode, and an Ag/AgCl electrode was utilized as the reference electrode. The cyclic voltametric (CV),

galvanostatic charge/discharge, and electrochemical impedance spectroscopic techniques were utilized to evaluate the electrochemical properties of the freshly prepared electrodes. An asymmetric supercapacitor (ASC) was fabricated with Ni_3Se_4/V_2C/rGO composite as the cathode, activated carbon as the anode, and Whatman® (grade 42) cellulose filter paper as the separator. The activated carbon electrode was fabricated following the same procedure used for the Ni_3Se_4/V_2C/rGO electrode. The ASC device was constructed in a split flat test cell for the evaluation of supercapacitor properties. The optimal mass loading ratio between the anode and cathode of the ASC device was calculated using equations (S1-2).

$$Q_+ = Q_- \quad \text{(S 1)}$$

$$\frac{m_+}{m_-} = \frac{C_- \times \Delta V_-}{C_+ \times \Delta V_+} \quad \text{(S 2)}$$

Here, m_+ and m_-; C_+ and C_-; and ΔV_+ and ΔV_- refer to the active material weight of the electrode, specific capacitance at 50 mV $s^{-1,}$ and potential window of the cathode and anode, respectively. The specific capacitance values (F g^{-1}) of the positive and negative electrodes were determined by Equation (S 3).

$$Csp = \frac{\int IdV}{SmV}, \quad \text{(S 3)}$$

where I denotes current density V refers to the voltage window, m signifies the weight of active electrode material and S denotes the scan rates. The specific capacity (C_s), specific capacitance (C_{sp}), energy density (E_{cell}) (WhKg^{-1}), and power density (P_{cell}) (WKg^{-1}) values were assessed by the Equations S (4-7), respectively.

$$C_s\,(mA\,h\,g^{-1}) = \frac{I \times \Delta t}{3.6 \times m} \quad \text{(S4)}$$

$$C_s\,(C\,g^{-1}) = \frac{I \times \Delta t}{m} \quad \text{(S5)}$$

$$C_{sp}\,(F\,g^{-1}) = \frac{I \times \Delta t}{m \times \Delta V} \quad \text{(S6)}$$

$$E_{cell} = \frac{1}{2 \times 3.6} \times C_{sp} \times \Delta V^2 \quad \text{(S7)}$$

$$P_{cell} = \frac{3600 \times E_{cell}}{\Delta t} \quad \text{(S8)}$$

where I, Δt, m, and ΔV signify the current density, discharge time , active electrode material weight, and voltage window, respectively.

The coulombic efficiency (η) is calculated using Equation (S8) :

$$\eta = {}^{t_D}/_{t_C} \times 100 \quad (S9)$$

where t_D and t_C are the discharging and charging times, respectively.

5. Electrode fabrication for HER analysis

A catalyst slurry was prepared by ultrasonically dispersing 5 mg of catalyst in 300 µL of DI water, 150 µL of isopropyl alcohol (IPA), and 50 µL of Nafion for 45 minutes. Subsequently, 15 µL of the resulting slurry was drop-cast three times onto pre-cleaned nickel foam. It was dried at 60°C for 10 h in a hot oven. Cyclic voltammetry (CV) and linear sweep voltammetry (LSV) were performed using three electrodes. The Ni_3Se_4, Ni_3Se_4/V_2C, Ni_3Se_4/rGO, and Ni_3Se_4/V_2C/rGO composites were used as the active electrode materials. The Hg/HgO and the Platinum foil were used as reference and counter electrodes, respectively. All tests were conducted at room temperature using a scan rate of 10 mV s^{-1}. The electrolyte solution was KOH (1.0 M, pH = 14), and it was purged with Ar gas for 30 minutes before the experiment. Before starting the electrochemical experiments, a few cycles were carried out continuously to stabilize the electrodes. All potentials are converted to a reversible hydrogen electrode (RHE) using Equation (S 9):

$$E\ (Vs\ RHE) = E\left(Vs\frac{Hg}{HgO}\right) + 0.0591\ (p^H + 0.105) \quad \text{(S9)}$$

Values are provided without *iR* correction. The kinetic Tafel plots (*log j vs* η_{10}) are derived from straight lines of least-squares fit in the Faradaic area, or CV (reverse sweep) plots. The measured current densities were standardized to the 1 ×0.5 cm^2 electrode geometric area. Electrochemical impedance spectroscopy (EIS) was carried out in the 10 Hz to 100 kHz

frequency range at -0.125 V vs RHE and 10 mV amplitude. Chronoamperometry (CA) study was utilized for the 24 h long-term stability analysis.

6. XRD analysis

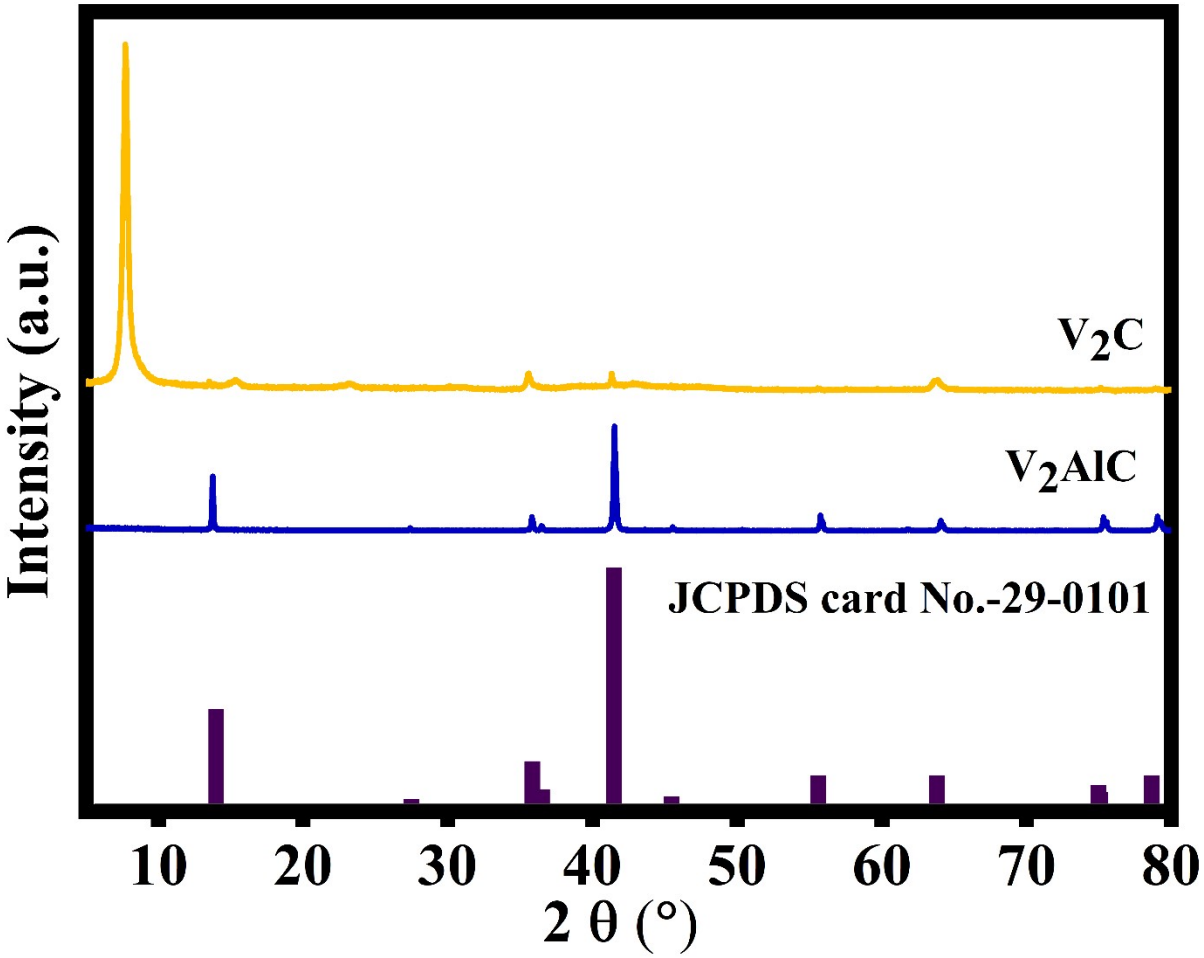

Figure S1: XRD analysis of V_2AlC and V_2C materials.

7. Raman Analysis

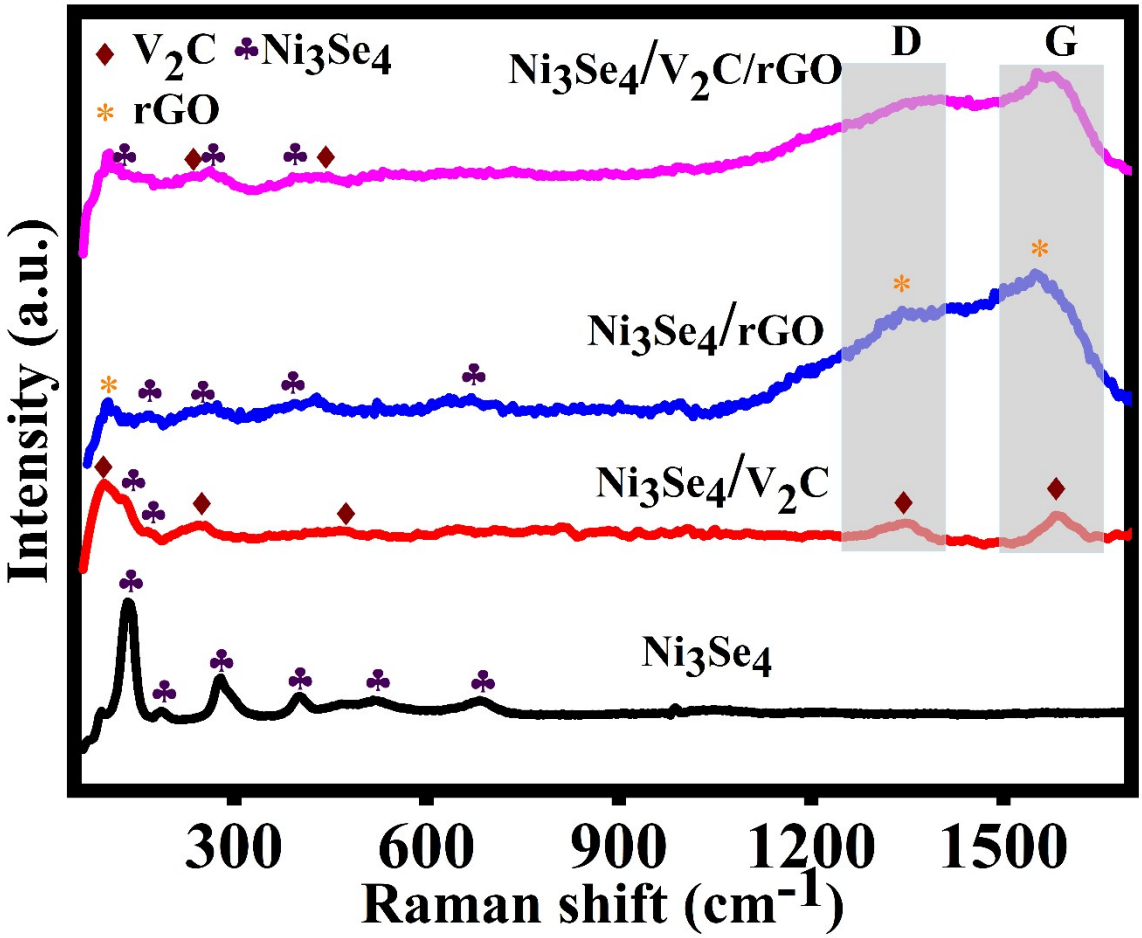

Figure S2: Raman analysis of Ni_3Se_4, Ni_3Se_4/V_2C, Ni_3Se_4/rGO and Ni_3Se_4/V_2C/rGO materials

8. XPS analysis

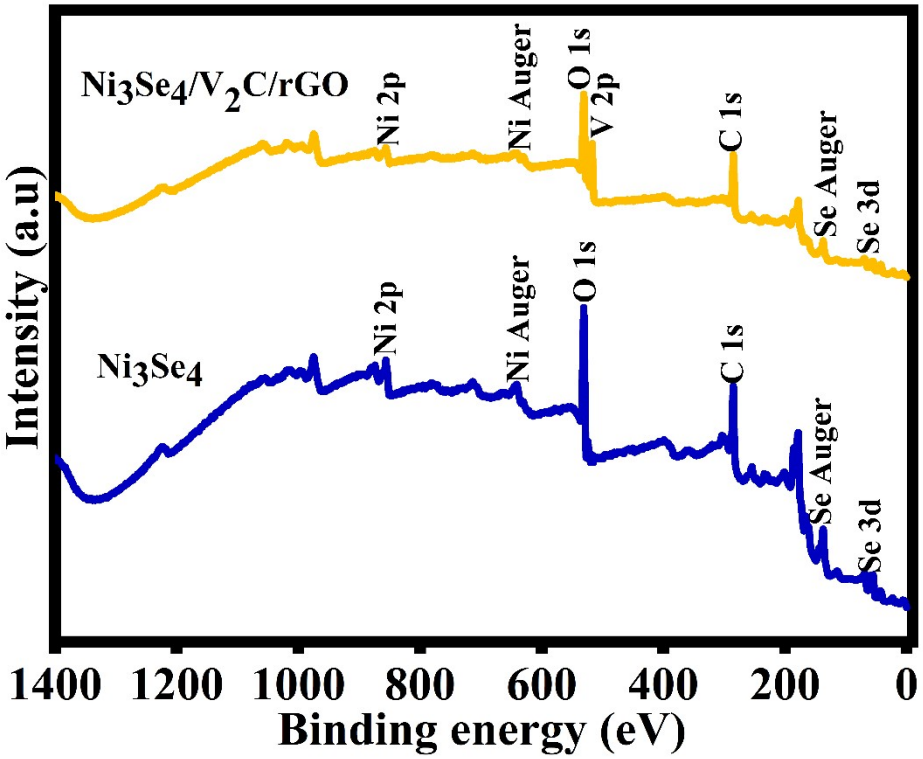

Figure S3: Survey spectra of the Ni_3Se_4 and Ni_3Se_4/V_2C/rGO materials.

9. BET analysis

Table S 2: BET analytic results

S. No	Materials	Specific surface area (m^2g^{-1})	Pore volume (cm^3g^{-1})	Pore size distribution (nm)
1	Ni_3Se_4	11.2356	0.0201	26
2	Ni_3Se_4/V_2C	13.1589	0.0205	32
3	Ni_3Se_4/rGO	14.2569	0.0203	36
4	Ni_3Se_4/V_2C/rGO	17.1879	0.0212	48
5				

10. SEM analysis

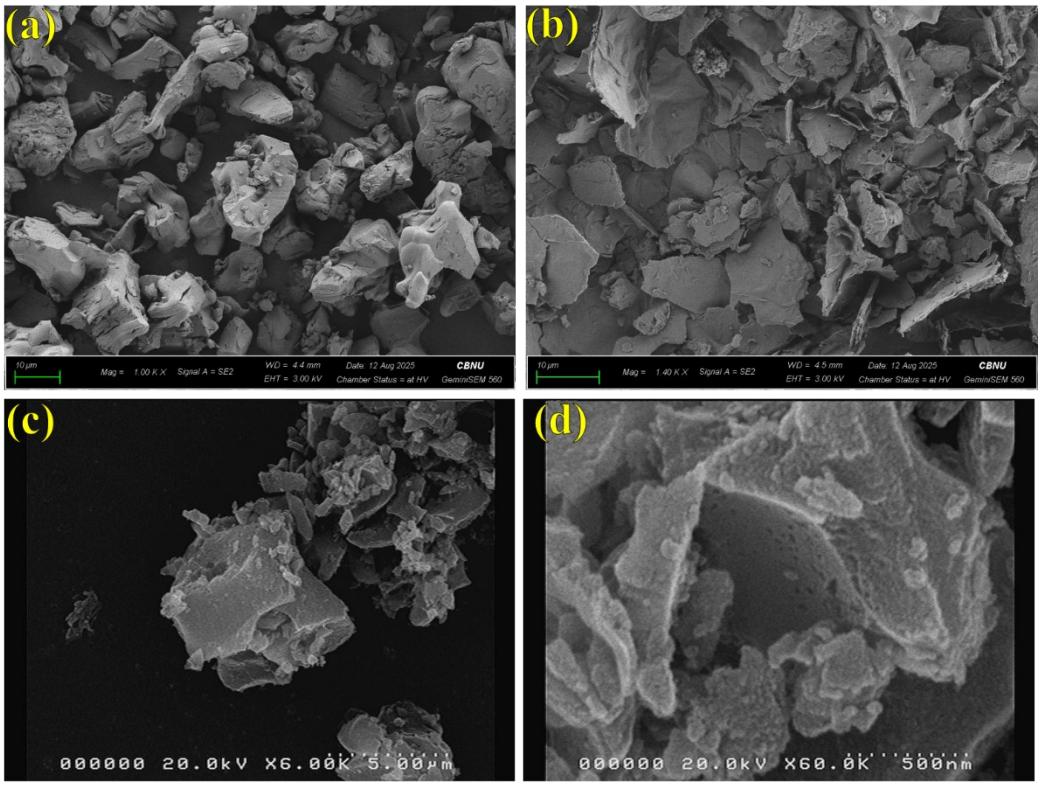

Figure S4: SEM analysis of (a) V_2AlC and (b) V_2C materials. (c) and (d) SEM analysis of activated carbon

11. TEM analysis

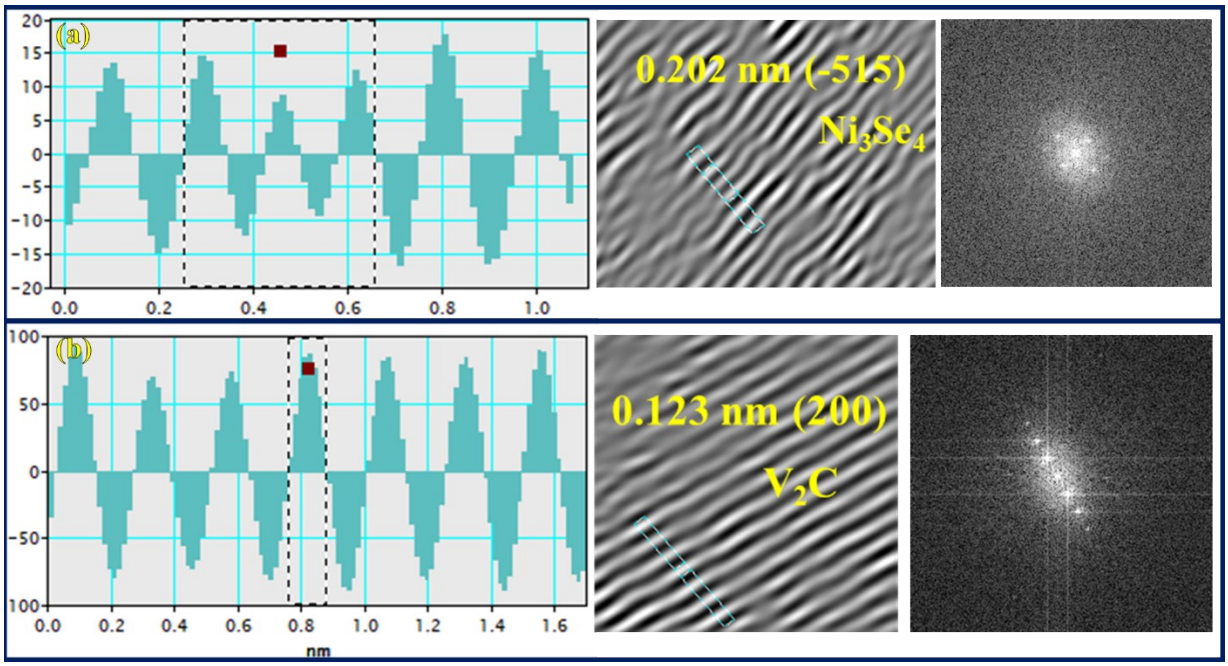

Figure S5: (a-b) line lattice fringes, fringes and masking FFT images of Ni_3Se_4/V_2C/rGO composite

12. Electrochemical supercapacitor analysis

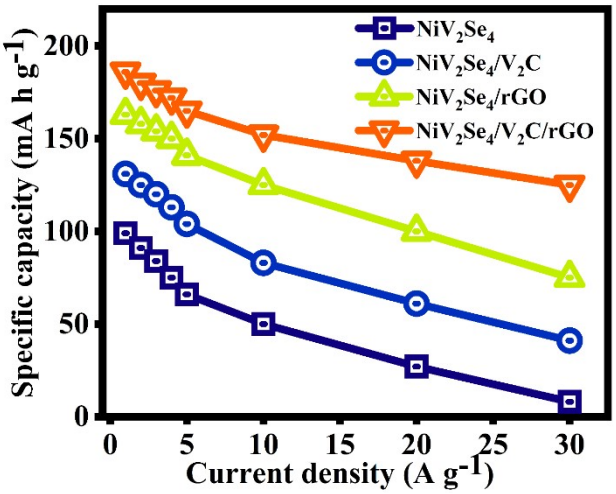

Figure S6: Rate capability graph of all electrodes

Table S 3: Supercapacitor performance comparison

S. No	Material	Electrolyte	Performance	Ref.
1	$NiSe_2$@CNT	6 M KOH	980.5 F g^{-1} at 1 A g^{-1}	[1]
2	NiCuSe	3 M KOH	127.2 mAh g^{-1} at 3 A g^{-1}	[2]
3	NiCoSe	3 M KOH	177.2 mAh g^{-1} at 3 A g^{-1}	[2]
4	$NiSe_2$	6 M KOH	744.7 F g^{-1} at 1 A g^{-1}	[3]
5	Ni–Co selenide /3D graphene/Ni foam	6 M KOH	742.4 F g^{-1} at 1 mA cm^{-2}	[4]
6	NiSe/NiO	1 M KOH	83.5 F g^{-1} at 2 mV s^{-1}	[5]
7	$NiCoSe_2$	3 M KOH	860 F g^{-1} at 2 mV s^{-1}	[6]
8	Activated carbon-decorated nickel diselenide	6 M KOH	119 C g^{-1} at 0.3 A g^{-1}	[7]
9	(Ni, Co)Se_2	2 M KOH	106 mAh g^{-1} at 1 A g^{-1}	[8]
10	**Ni_3Se_4/V_2C/rGO**	**2 M KOH**	**186 mAh g^{-1} at 1 A g^{-1}** **1031 F g^{-1} at 1 A g^{-1}** **670 C g^{-1} at 1 A g^{-1}**	**Present work**

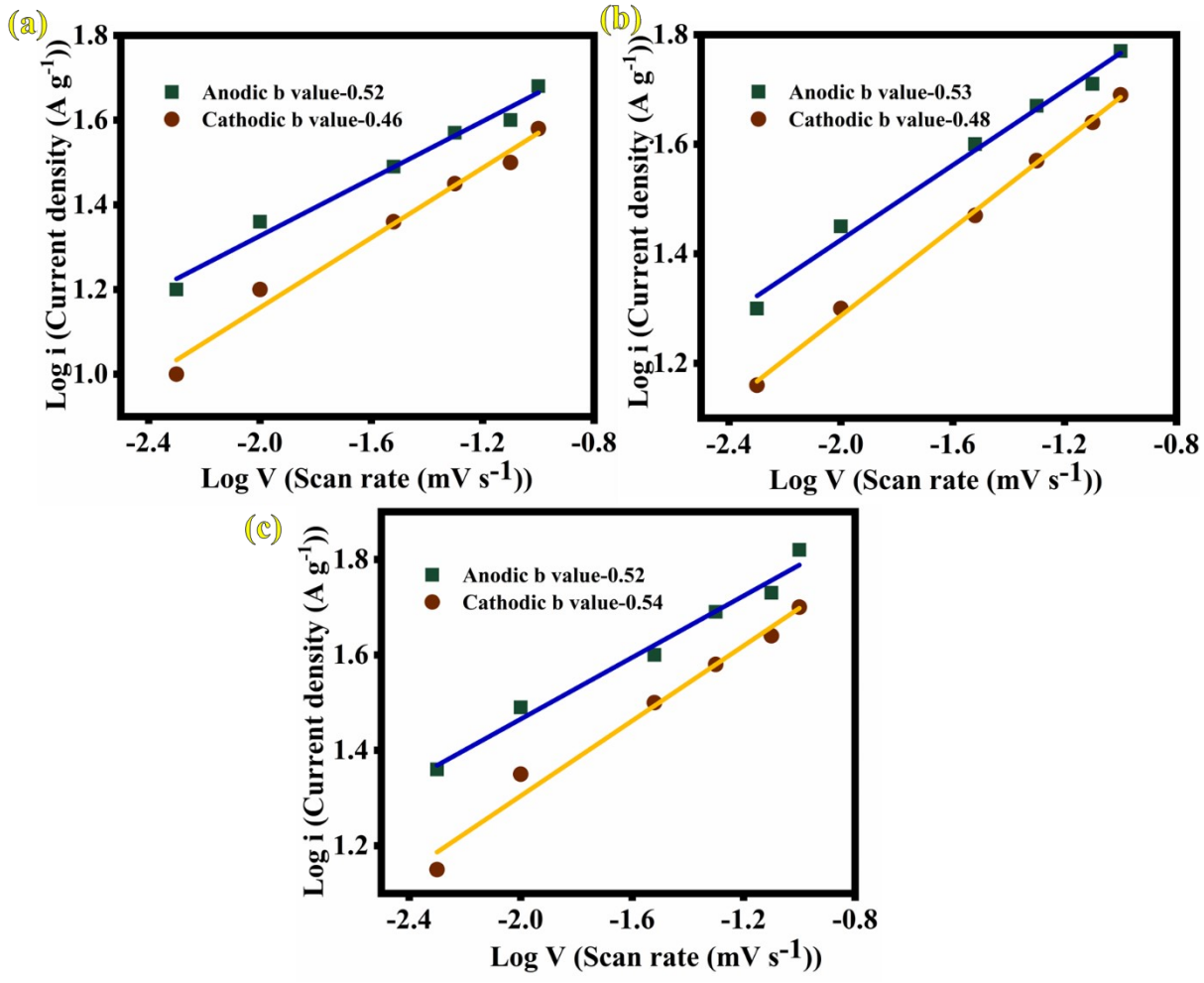

Figure S 7: Logarithmic plots of (a) Ni_3Se_4/V_2C, (b) Ni_3Se_4/rGO and (c) Ni_3Se_4/V_2C/rGO electrodes

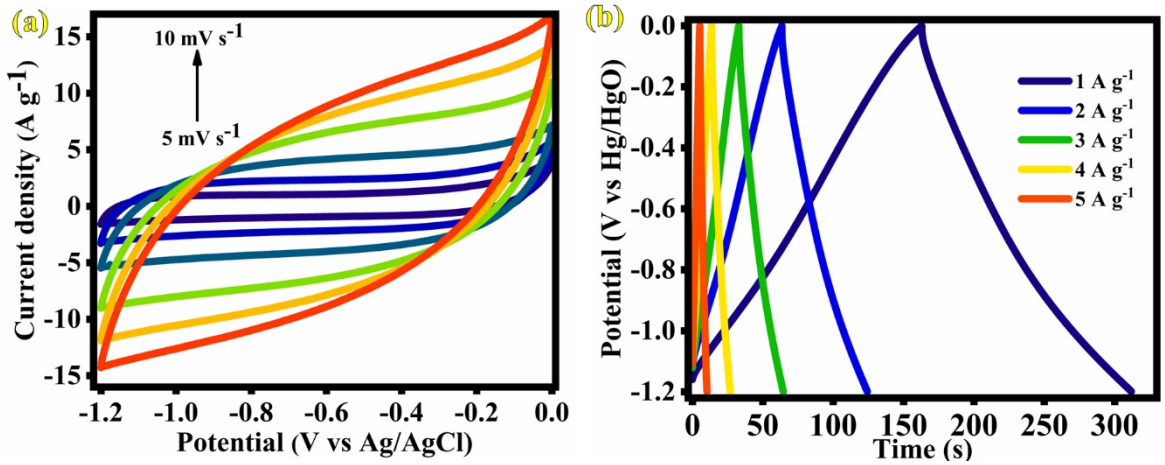

Figure S8: (a) CV and (b) GCD analyses of AC material

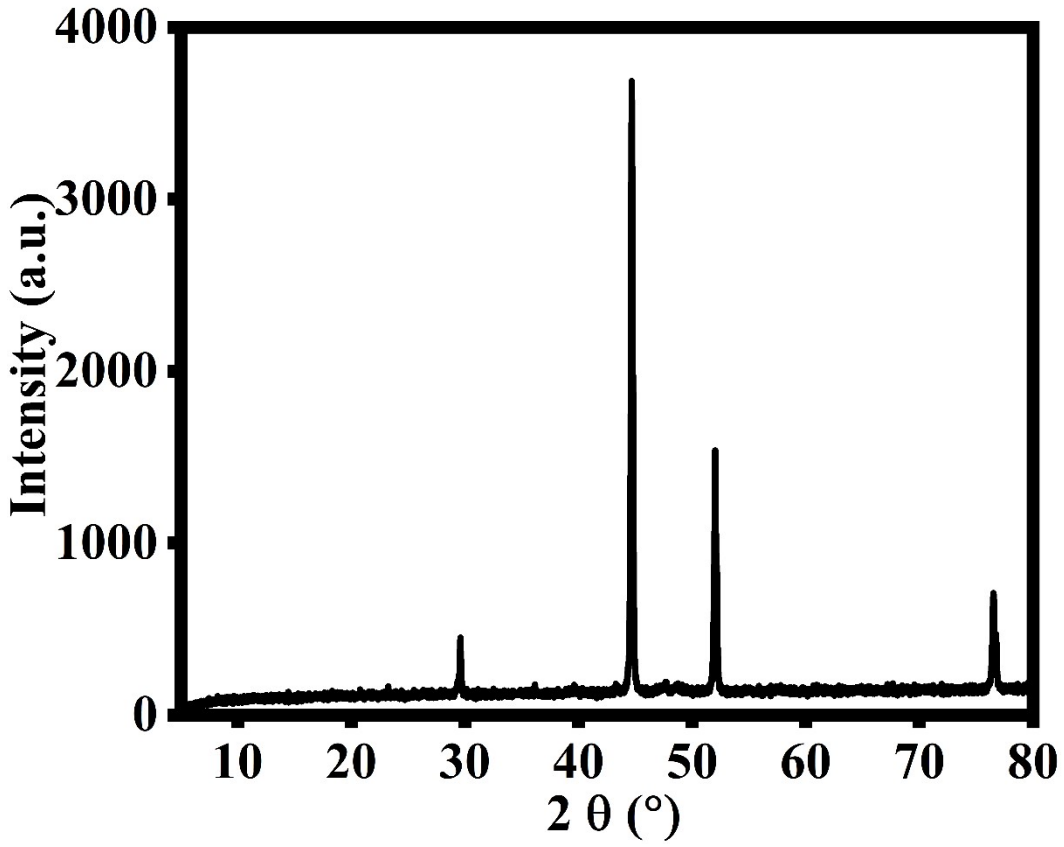

Figure S9: XRD analysis after cyclic stability studies

13. HER analysis

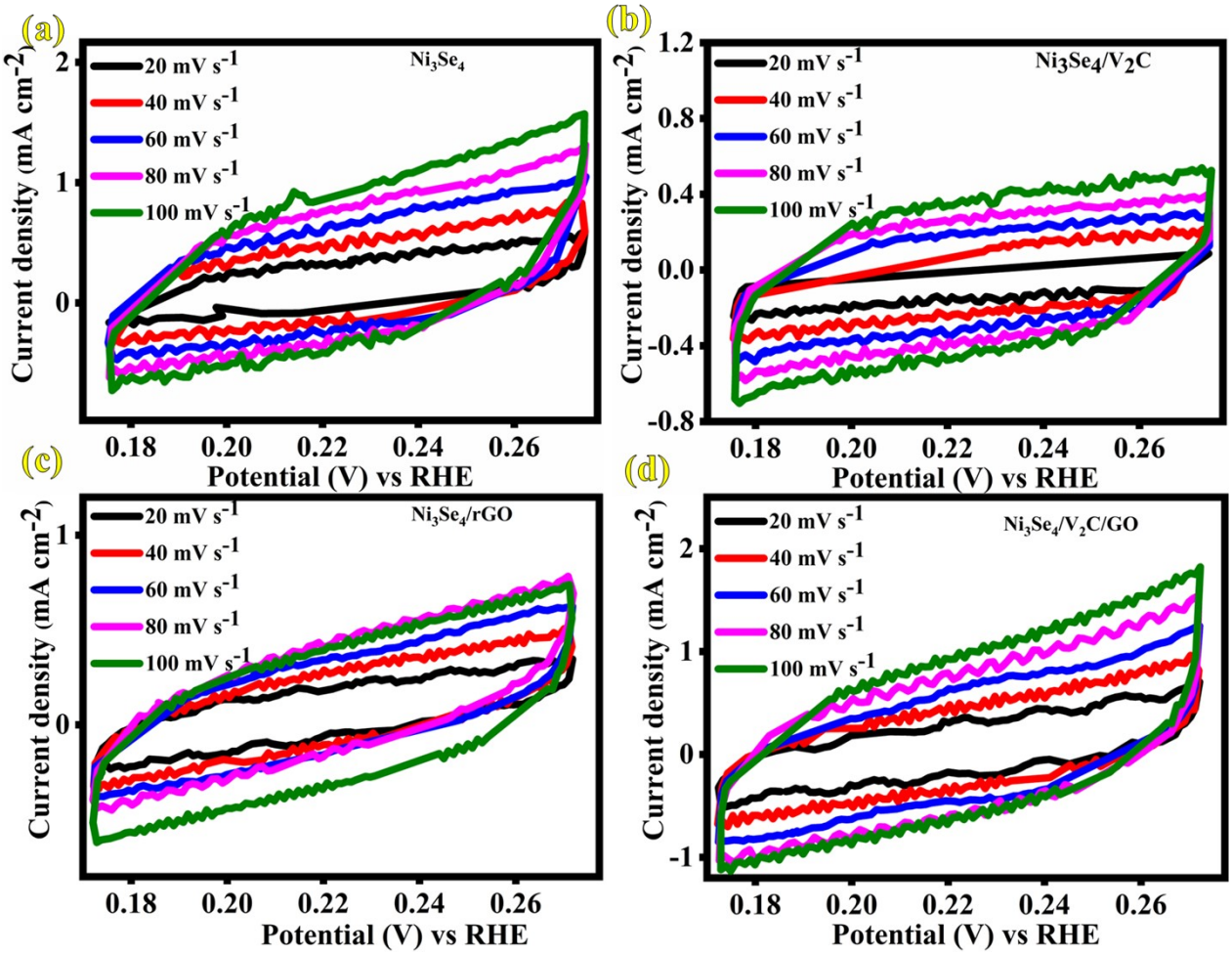

Figure S10: ECSA analysis of (a) Ni_3Se_4, (b) Ni_3Se_4/V_2C, (c) Ni_3Se_4/rGO, and (d) Ni_3Se_4/V_2C/rGO electrodes

Table S4: Comparison for HER performance

Electrocatalyst	**Electrolyte**	**Overpotential (η_{10})**	**Tafel (mV/dec)**	**Stability (hours)**	**Ref.**
Co_7Se_8/MXene	1.0 M KOH	270	128.5	24	[9]
$Ni_{0.9}Fe_{0.1}PS_3$@MXene	1.0 M KOH	196	114	50	[10]
NiS_2/V-MXene	1.0 M KOH	179	85	4	[11]
P_3–V_2CT_x	0.5 M H_2SO_4	163	28	25	[12]
$MoSe_2$/MXene–O	0.5 M H_2SO_4	171	61	10	[13]
VS_2@V_2C	1.0 M KOH	164	47.6	200	[14]
Fe_d-NiS_2/MXene	1.0 M KOH	148	85	60	[15]
$CoSe_2$ and WSe_2	1.0 M KOH	157	79	12	[16]
NC-$NiSe_2$	0.5 M H_2SO_4	127	84	48	[17]
Ni_2Se_3/V_2C/rGO	**1.0 M KOH**	**118.3**	**112**	**24**	**Present work**

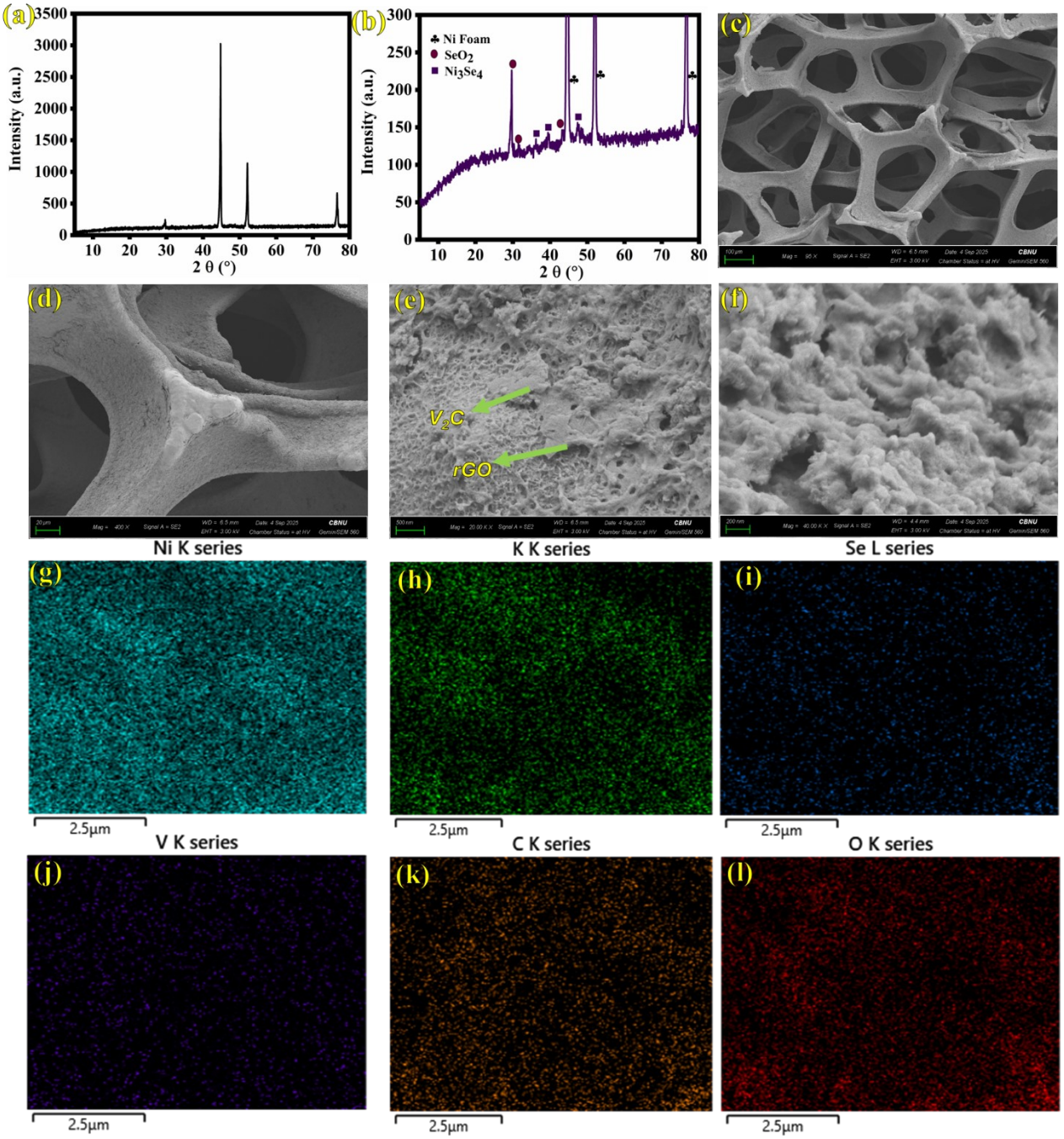

Figure S11: Post studies of Ni_2Se_3/V_2C/rGO. (a) XRD, (b) enlarged XRD, (c-f) SEM analysis and (g-l) elemental mapping analysis.

References

1 Y. Zheng, Y. Tian, S. Sarwar, J. Luo and X. Zhang, *J. Power Sources*, 2020, **452**, 227793.

2 K. K. Garlapati, A. R. Nath, A. M. Arjun, A. Vijayan and N. Sandhyarani, *Electrochim. Acta*, 2022, **424**, 140627.

3 M. Aftabuzzaman and H. K. Kim, *Mater. Chem. Phys.*, 2025, **329**, 130052.

4 Y. Wang, W. Zhang, X. Guo, K. Jin, Z. Chen, Y. Liu, L. Yin, L. Li, K. Yin, L. Sun and Y. Zhao, *ACS Appl. Mater. Interfaces*, 2019, **11**, 7946–7953.

5 K. S. Bhat and H. S. Nagaraja, *Mater. Res. Express*, 2018, **5**, 105504.

6 S. Saranya, S. Suthakaran, S. Dhanapandian, A. Dinesh, R. P. Patil, M. Ayyar, L. Gnanasekaran and S. Santhoshkumar, *Results Chem.*, 2025, **13**, 102009.

7 S. Tanwar, N. Singh and A. L. Sharma, *J. Mater. Sci.*, 2022, **57**, 20335–20350.

8 H. Lei, J. Zhou, R. Zhao, H. Peng, Y. Xu, F. Wang, H. A. Hamouda, W. Zhang and G. Ma, *Electrochim. Acta*, 2020, **363**, 137206.

9 N. C. S. Selvam, J. Lee, G. H. Choi, M. J. Oh, S. Xu, B. Lim and P. J. Yoo, *J. Mater. Chem. A Mater.*, 2019, **7**, 27383–27393.

10 C. Du, K. N. Dinh, Q. Liang, Y. Zheng, Y. Luo, J. Zhang and Q. Yan, *Adv. Energy Mater.*, DOI:10.1002/aenm.201801127.

11 P. Kuang, M. He, B. Zhu, J. Yu, K. Fan and M. Jaroniec, *J. Catal.*, 2019, **375**, 8–20.

12 Y. Yoon, A. P. Tiwari, M. Choi, T. G. Novak, W. Song, H. Chang, T. Zyung, S. S. Lee, S. Jeon and K. An, *Adv. Funct. Mater.*, DOI:10.1002/adfm.201903443.

13 W. Xiao, D. Yan, Y. Zhang, X. Yang and T. Zhang, *Energy & Fuels*, 2021, **35**, 4609–4615.

14 Z. Wang, W. Xu, K. Yu, Y. Feng and Z. Zhu, *Nanoscale*, 2020, **12**, 6176–6187.

15 Y. Zhao, Y. Zhu, C. Xi, K. Hu, S. Han and J. Jiang, *Applied Catalysis B: Environment and Energy*, 2025, **378**, 125611.

16 M. Muska, J. Yang, Y. Sun, J. Wang, Y. Wang and Q. Yang, *ACS Appl. Nano Mater.*, 2021, **4**, 5796–5807.

17 S. He, B. Chen, C. Meng, F. Shi, A. Yuan, W. Miao and H. Zhou, *ACS Appl. Nano Mater.*, 2024, **7**, 1138–1145.